Spectrochimica Acta Part A: Molecular and Biomolecular Spectroscopy 303 (2023) 123133

Contents lists available at ScienceDirect

Spectrochimica Acta Part A:
Molecular and Biomolecular Spectroscopy

journal homepage: www.journals.elsevier.com/spectrochimica-acta-part-a-molecular-and-biomolecular-spectroscopy

A study of major cannabinoids via Raman spectroscopy and density functional theory

Trevor J. Wolfe [a], Nicholas A. Kruse [a], Mohamed M. Radwan [b], Amira S. Wanas [b], Kalee N. Sigworth [a], Mahmoud A. ElSohly [b,c], Nathan I. Hammer [a,*]

[a] Department of Chemistry and Biochemistry, University of Mississippi, Coulter Hall, University, MS 38677, USA
[b] National Center for Natural Products Research, School of Pharmacy, University of Mississippi, University, MS 38677, USA
[c] Department of Pharmaceutics and Drug Delivery, School of Pharmacy, University of Mississippi, University, MS 38677, USA

HIGHLIGHTS

- Raman spectra of a series of eleven cannabinoids are presented and compared.
- Experimental results are compared to simulated spectra from density functional computations.
- The spectra are very resolved experimentally and are highest-level simulated spectra available to date for each cannabinoid.
- Deviations between experiment and theory are observed in the OH-stretching regions are likely due to hydrogen bonding.

GRAPHICAL ABSTRACT

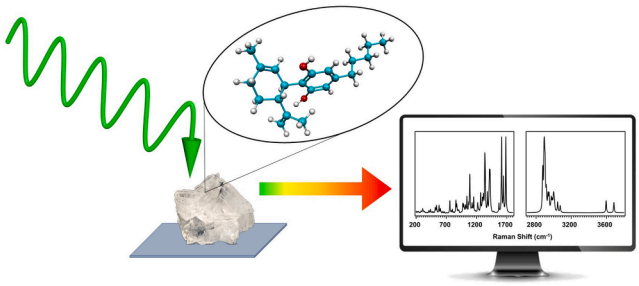

ARTICLE INFO

Keywords:
Cannabinoids
Raman spectroscopy
Computational chemistry
M06-2X
Density functional theory

ABSTRACT

Cannabinoids, a class of molecules specific to the cannabis plant, are some of the most relevant molecules under study today due to their widespread use and varying legal status. Here, we present Raman spectra of a series of eleven cannabinoids and compare them to simulated spectra from density functional theory computations. The studied cannabinoids include three cannabinoid acids (Δ^9-THC acid, CBD acid, and CBG acid) and eight neutral ones (Δ^9-THC, CBD, CBG, CBDVA, CBDV, Δ^8-THC, CBN and CBC). All cannabinoids have been isolated from cannabis plant gown at the University of Mississippi. The data presented in this work represents the most resolved experimental and highest-level simulated spectra available to date for each cannabinoid. All cannabinoids displayed higher peak separation in the experimental spectra than CBGA, which is most likely attributable to physical composition of the samples. The overall agreement between the experimental and simulated spectra is good, however for certain vibrational modes, especially those in the –OH stretching region, deviations are observed due to hydrogen bonding, suggesting that the OH stretching region is a good probe for decarboxylation reactions in these and related species.

* Corresponding author.
E-mail address: nhammer@olemiss.edu (N.I. Hammer).

https://doi.org/10.1016/j.saa.2023.123133
Received 13 February 2023; Received in revised form 2 June 2023; Accepted 10 July 2023
Available online 11 July 2023

1. Introduction

Cannabis plant (*Cannabis sativa*) has been cultivated by humans for about 4,000 years and is known for its various effects on the mind [1,2]. Its changing legal status makes cannabis usage a heavily studied topic in recent years. In 2017, two research teams, one on each coast of the United States, found that 6% of middle schoolers, 24% of high schoolers, and 21% of adults aged 18–34 reported cannabis usage in the past year [3–5]. Additionally, new therapeutic effects for the treatment of diseases such as multiple sclerosis, chronic pain, and glaucoma are consistently being discovered [6].

Regarding the constituents of the plant itself, cannabis is a complex mixture of over 500 compounds, of which more than 100 are cannabinoids [7,8]. The major cannabinoids found in cannabis include: cannabidiol (CBD), Δ^9-*trans*-tetrahydrocannabinol (Δ^9-THC), Δ^8-*trans*-tetrahydrocannabinol (Δ^8-THC), cannabigerol (CBG), cannabichromene (CBC), and cannabinol (CBN), all of which have various subtypes of each cannabinoid in addition to their most commonly observed structure, such as their acidic and varinic counterparts [8]. All cannabinoids studied in this work are biosynthetically originated from cannabigerolic acid (CBGA), the central cannabinoid precursor [9], or are structurally very similar. As shown by the biosynthetic pathways depicted in Fig. 1, CBGA is enzymatically converted to Δ^9-THCA, cannabidiolic acid (CBDA) and cannabichromenic acid (CBCA) [10]. Each of these compounds is then non-enzymatically decarboxylated to their corresponding neutral cannabinoids, CBG, Δ^9-THC, CBD, and CBC, respectively. Further conversion involves the isomerization of Δ^9-THC into Δ^8-THC, which can subsequently be oxidized to CBN. The closely related cannabidivarinic acid (CBDVA) and cannabidivarin (CBDV) that are biosynthetically originated from cannabigerovarinic acid (CBGVA) are also included in this study (Fig. 1).

While there are other conversion processes and compounds involved in this biosynthetic pathway, they go beyond the scope of this current study. As can be expected, the structural differences between the

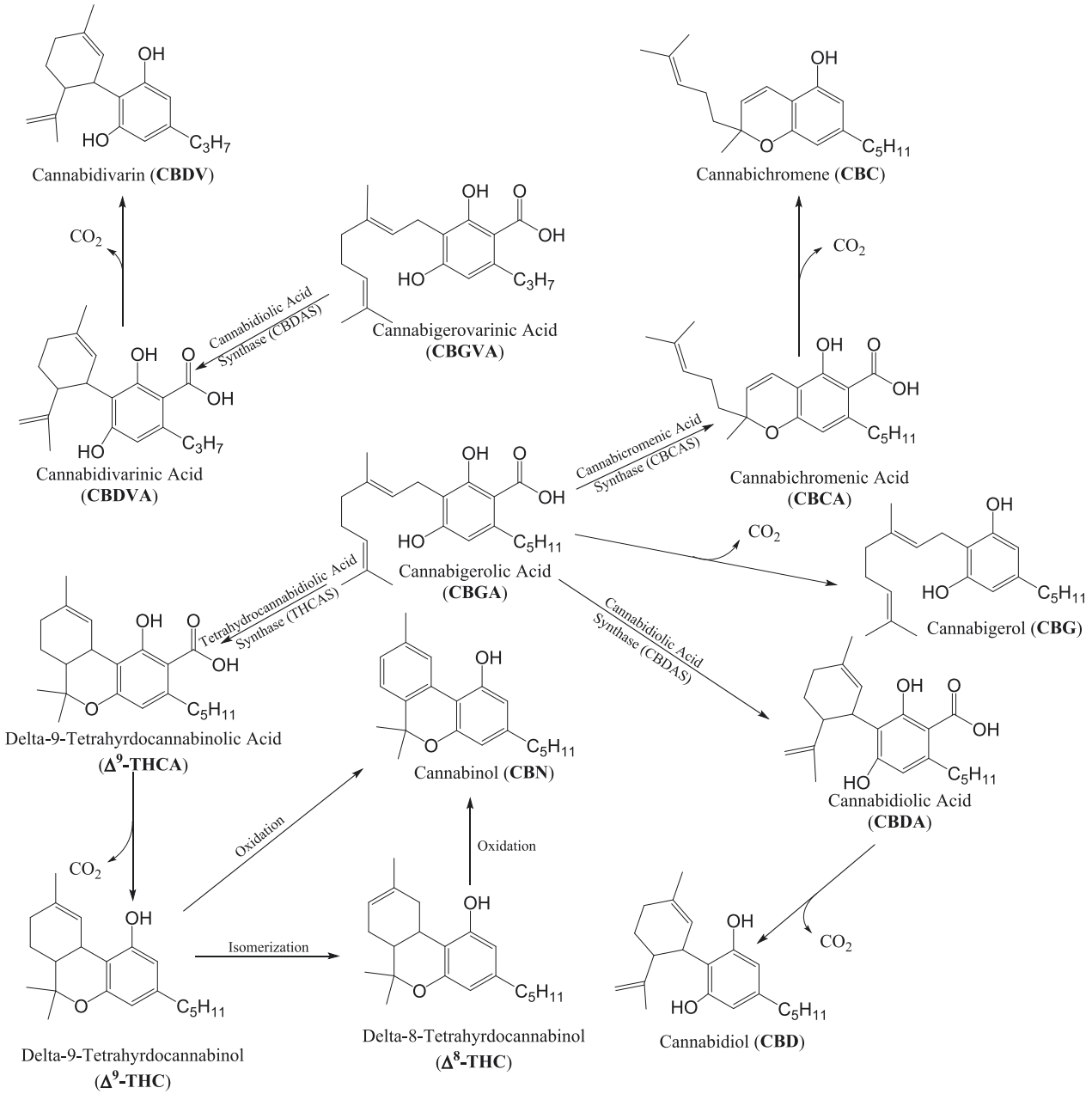

Fig. 1. Biosynthesis of cannabinoid acids and formation of neutral cannabinoids.

different cannabinoids produce different effects when used. For instance, unlike Δ^9-THC, CBG does not produce any psychotropic effects, however it demonstrates antibacterial properties against gram positive bacteria [8]. Additionally, although the only structural difference between Δ^8- and Δ^9-THC is the location of a double bond in the cylcohexene ring, Δ^8-THC is less psychoactive than Δ^9-THC, giving rise to a varying legal status across different states and countries [11,12].

Raman spectroscopy has been used to study various properties of cannabis, such as hydrogen bonding activities, cannabinoid content in various strains, spectral library creation, illicit drug sample analysis, and even synthetic cannabinoid characterization [13–31]. However, in these studies containing experimental Raman spectra of cannabinoids, the range in which the spectra are presented is extremely narrow, typically only 700–1800 cm^{-1}. Moreover, in cases where handheld Raman spectrometers were employed, the spectral data is limited by relatively low resolution (~9–18 cm^{-1}) [14,15,23]. The work described herein improves upon the current data by employing a higher resolution benchtop Raman spectrometer to record the spectra over a broader range to include as many peaks as are present for each sample. While full experimental data files are included in Appendix A, abridged plots showcasing the fingerprint and stretching regions are presented herein.

While some have also attempted to use computational chemistry to assign spectral features in cannabinoids, there are few examples of comparing full simulated Raman spectra to experimental spectra [16,32]. However, there are more examples of computational chemistry being used to study cannabinoids for a variety of other applications, such as to determine their antioxidant activity, calculate theoretical chemical and thermodynamic properties, and more [33–42]. While the chosen method and basis set varies throughout the existing literature, the use of density functional theory (DFT) is consistent due to its reasonably high accuracy and relatively low computational cost [43]. These two aspects make DFT an especially appealing choice for studying cannabinoids, as the large size of each molecule would incur a larger computational cost with other methods. As such, DFT is utilized to perform all computational studies described herein.

2. Materials and methods

2.1. Sample preparation and isolation of cannabinoids

Cannabis of different varieties (High THC, High CBD, High CBG and THC/CBD) were grown at the University of Mississippi. Upon maturation, the buds were harvested and dried using forced hot air. The dried buds were ground and kept at −20 °C. High THC plant material was used to isolate Δ^9-THC acid, Δ^9-THC, CBC, CBG, CBG acid and CBN. The high CBD variety was used to isolate CBD acid, CBD, and CBDV. The purity of the isolated cannabinoids is more than 95%.

2.1.1. Isolation of Δ^9-THC acid, Δ^9-THC, CBC, CBG, CBG acid and CBN

The powdered cannabis plant material of high THC variety was extracted with hexanes, CH_2Cl_2, EtOAc, EtOH, EtOH/H_2O (1:1), and H_2O at room temperature. The hexanes extract was dried under reduced pressure at 40 ^{0}C, then chromatographed over silica gel vacuum liquid chromatography and flash chromatography columns eluted with gradient EtOAc/hexanes. The column fractions rich in cannabinoids were purified using semipreparative C_{18}-HPLC to afford Δ^9-THC acid, Δ^9-THC, CBC, CBG, CBG acid and CBN [44–46].

2.1.2. Isolation of CBD acid, CBD, and CBDV

Dried High CBD variety cannabis material was extracted with hexanes and the dried hexane extract was chromatographed on a silica gel column chromatography eluted with 2% EtOAc/hexanes. The CBD rich column fraction was crystallized from hexanes to give pure CBD as white crystals. CBDA was isolated from the polar column fractions using C18-solid phase extraction (SPE) and isocratically eluted with 75% Acetonitrile/Water. The CBDV rich column fraction was chromatographed on C18-semipreprative HPLC using 73% Acetonitrile/Water to give pure CBDV as a white powder.

2.1.3. Preparation of Δ^8-THC

Δ^8-THC was prepared by acid catalyzed cyclization of CBD as following: CBD (40 mg) was dissolved in 5 mL of CH_2Cl_2 and *p*-toluenesulfonic acid (0.4 mg) was added. The mixture was refluxed for 3 h, after cooling down the reaction mixture was neutralized with 10% sodium bicarbonate solution. Pure Δ^8-THC (35 mg) was separated as a light brown oil after the evaporation of the organic layer [47].

2.2. Raman spectroscopy

All experimental spectra presented were collected using a LabRAM HR Evolution Raman Spectrometer (Horiba Scientific, Kyoto, Japan) equipped with a charge-coupled device (CCD) camera detector and a 600 grooves/mm diffraction grating. For the spectra presented herein, a 50X LWD objective lens was utilized with a spot size of 64 μm^2. We initially employed a variety of objectives for the microRaman studies and saw little if no differences in spectral features when using different magnifications, focusing, or sample locations. The samples were excited using a 532 nm Nd:YAG laser (Oxxius, Lannion, France). With this instrumental setup, spectral resolution of less than 1 cm^{-1} can be achieved. Each spectrum was acquired under the following parameters: 50 accumulations, an acquisition time of 2 s, and an aperture size of 100 μm. To ensure calibration of the spectrometer, the spectrum of a crystalline Si wafer with a known Raman band at 520 cm^{-1} was recorded prior to analysis of the samples. The spectra range from 200 to 4000 cm^{-1}, however they are presented here in an abridged form to highlight the peaks of interest.

2.3. Computational chemistry

Using the *Gaussian 16* software suite, the geometry of each molecule is optimized and the harmonic frequencies are calculated [48]. Due to the rather large size of the cannabinoids, density functional theory (DFT) calculations are performed using the M06-2X method [49] and the aug-cc-pVTZ basis set [50]. The complexity of the molecules prevents a thorough conformational analysis, and it is beyond the scope of this work to guarantee that all minima were global. To account for anharmonicity and intermolecular interactions in condensed phases, these frequencies are subsequently multiplied by an empirically determined scaling factor of 0.95. Utilizing the calculated harmonic frequencies and Raman activities, Lorentzian profiles are constructed and summed in order to produce the simulated spectra. As with the experimental spectra, the simulated spectra are abridged to highlight the peaks of interest.

3. Results and discussion

3.1. CBG pathway – CBGA and CBG

Beginning with CBGA, the cannabinoid from which all others studied here are derived, a quick comparison of Fig. 2 (experimental Raman spectrum) with Fig. 3 (simulated spectrum) suggests poor agreement. One of the clearest differences can be seen in the –OH stretching region. Whereas the simulated spectrum predicts three distinct peaks at 3536, 3608, and 3688 cm^{-1}, which come from the carboxylic –OH as well as the two –OH groups present on the terpene ring, the experimental spectrum shows a single broad.

peak centered at 3705 cm^{-1}. This discrepancy likely arises because the simulated spectrum only accounts for a single molecule in an isolated environment, and as such cannot accurately depict the effects of inter- and intra-molecular hydrogen bonding, which create a band broadening effect that obscures two of the peaks. This conclusion is further supported by the blue shift (increase) in energy of the –OH

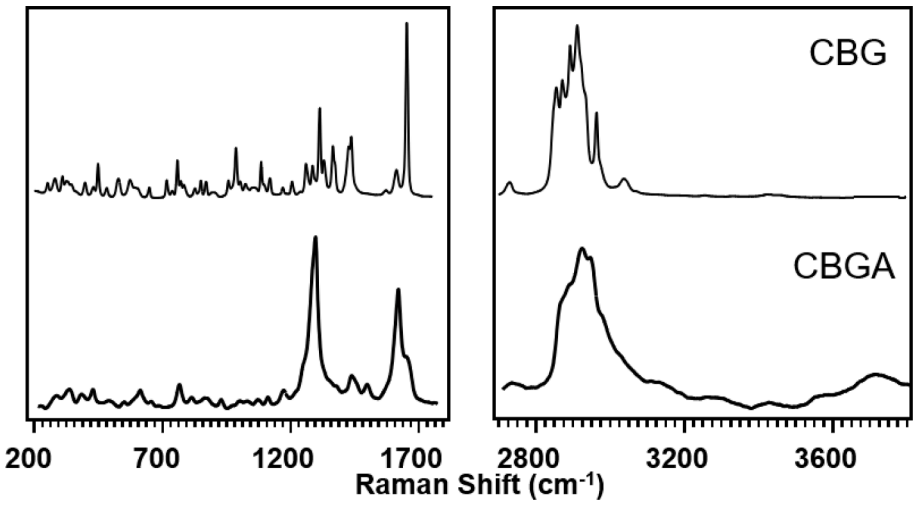

Fig. 2. Experimental Raman Spectra of CBG Pathway.

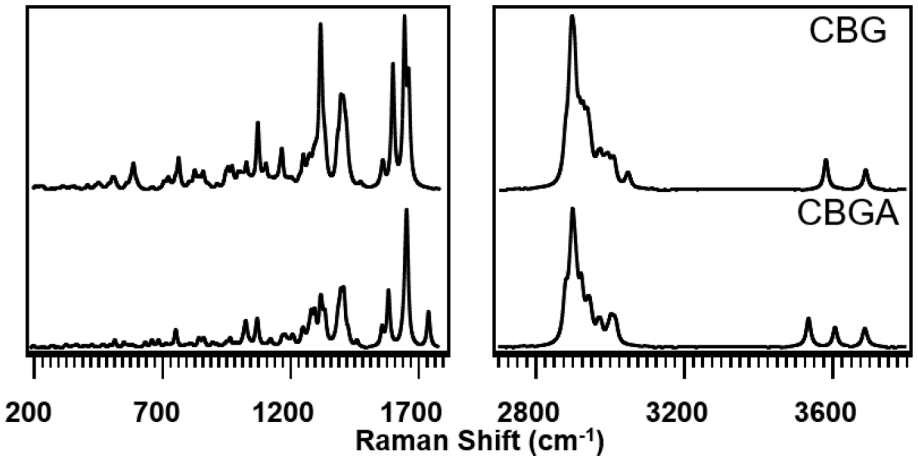

Fig. 3. Simulated Raman Spectra of CBG Pathway.

vibrational modes in the experimental spectrum as compared to its simulated (in isolation) counterpart. There is, however, better agreement in the CH stretching region in terms of the Raman shift: the simulated spectrum predicts the most intense peak at 2899 cm^{-1}, while in the experimental spectrum it is located at 2911 cm^{-1}. Still, only two peaks are discernable in the experimental spectrum where the simulated spectrum predicts five. This is most likely due to the oily nature of the sample, which could cause band broadening as opposed to the calculations performed in isolation. Like with the functional group region of the spectrum, the fingerprint region does not demonstrate a high degree of agreement between experiment and theory. For instance, the simulated spectrum contains three intense peaks at 1602, 1671, and 1760 cm^{-1}, while the experimental spectrum shows one distinct peak at 1622 cm^{-1} with a shoulder on the right side. As with the –OH and –CH stretching regions, the increased rotational freedom inherent in the oily sample most likely leads to the band broadening witnessed in this region of the experimental spectrum. Additionally, the intense peak at 1297 cm^{-1} does not have an immediately clear analog in the simulated spectrum. It is possible that this band represents the peaks at either 1295 or 1308 cm^{-1}, but due to its broadness it is difficult to say which one. While the rest of the spectrum shows much better agreement between experiment and theory, overall the agreement is less than ideal.

After thermal decarboxylation, CBGA loses its carboxylic acid moiety and becomes CBG. Thus, it is expected that the Raman spectrum of CBG will be very similar to that of CBGA, with the greatest difference occurring in the –OH stretching region. This expectation is shown to be accurate in Fig. 3, where in the simulated spectrum, CBG has only two –OH peaks compared to CBGA's three. However, the experimental spectrum depicts a significantly weaker, less broad band compared to that of CBGA at 3425 cm^{-1}. Since this peak is also red-shifted compared to the simulated spectrum, it is theorized that CBG does not participate in hydrogen bonding to the same extent as CBGA, meaning that most of the hydrogen bonding in CBGA likely occurs through the carboxylic acid moiety. In the –CH stretching region, the simulated spectrum closely resembles that of CBGA. In both, the most intense peak is skewed towards the left side of the band, with roughly the same width and a less intense peak to the right. The main difference is the narrower and less intense band for CBG as compared to CBGA. Additionally, better agreement is seen between experiment and theory in this region for CBG, where the most intense experimental peak is of comparable width with the most intense portion blue-shifted and the entirety of the band slightly redshifted. In this region, a significant increase in peak separation is seen for the experimental spectrum compared to that of CBGA and even the simulated spectrum which most likely arises from the crystalline nature of the CBG sample as opposed to the liquid, oily nature of the CBGA sample. Finally, in the fingerprint region, even better agreement between experiment and theory is seen than is shown in the spectra for CBGA. Comparing the two compounds' spectra, there is a noticeable lack of an intense peak at 1297 cm^{-1} in the experimental spectrum for CBG. This peak in CBGA is associated with carbonyl stretching in the

carboxylic acid group, so differences between the spectra in this region can be attributed to CBG's lack of a carbonyl group. Overall, the agreement between the simulated and experimental spectra is much better for CBG than for CBGA, with the most notable differences explained by the loss of the carboxylic acid moiety.

3.2. CBD pathway – CBDA, CBD, CBDVA, and CBDV

Moving on to the CBD biosynthetic pathway, cannabidiolic acid synthase (CBDAS) converts CBGA and CBGVA into CBDA and CBDVA, respectively, which are subsequently decarboxylated into CBD and CBDV, respectively[9]. The experimental and simulated Raman spectra of these molecules are shown in Figs. 4 and 5, respectively. The simulated spectrum for CBDA possesses three –OH stretching vibration peaks similar to those of CBGA, the most intense of which is associated with the –OH group on the carboxylic acid group while the other two represent other –OH groups. However, one is closer in energy to the –CH stretching region, which is possibly the result of intramolecular hydrogen bonding. In the –CH stretching region, the highest-energy, two-peak band is not present in the simulated spectrum of CBGA, and the spectrum possesses less separation between the most intense peaks. These differences are believed to arise from the cyclization of the terpene tail of CBGA into the monoterpene ring of CBDA. Moving to the fingerprint region, vibrational modes, specifically those around 1700 cm^{-1}, differ considerably. While the carbonyl (1760 cm^{-1}) and C═C (1671 cm^{-1}) stretching modes are well resolved for CBGA, the bands are much closer in CBDA to the point where they overlap at 1659 cm^{-1}. Additionally, the red shift in energy for the C═C stretching mode in the terpene tail suggests that the cyclization of the terpene tail stabilizes the overall molecule, which also potentially explains the red shift in the carbonyl stretching mode energy.

In the experimental spectrum, higher peak separation and stronger agreement is seen between experiment and theory for CBDA as opposed to CBGA. The greatest difference between the experimental spectra for CBDA and CBGA is the broad, intense band centered at 3856 cm^{-1} in the spectrum for CBDA, indicating an increase in hydrogen bonding. The separate –OH stretching band at 3410 cm^{-1}, while lower in intensity, does correspond to the second band seen in the simulated spectrum for CBDA, with the decrease in intensity indicating less hydrogen bonding than the band centered at 3856 cm^{-1}. In the –CH stretching region, the eight resolved peaks in the simulated spectrum become five experimentally, indicating band broadening. While the simulated spectrum predicts a greater difference between CBDA and CBGA, the experimental spectrum shows more commonality, mainly in the carbonyl and C═C stretching modes but also in the –CH stretching region to a lesser extent. The only experimentally verifiable difference between CBDA and CBGA is the separation in –OH vibrational modes. While these spectra have the highest resolution seen in the literature, greater peak separation (mainly from taking spectra of CBGA in the solid state) could further distinguish between the two molecules experimentally to match their differences seen in theory.

CBDA undergoes decarboxylation to form CBD, the simulated spectrum of which reveals that the greatest differences between CBDA and CBD occur in the hydroxyl and carbonyl vibrational modes. The carboxylic acid –OH vibrational mode is not present, the energy difference between the phenolic –OH vibrational modes is not as great in CBD as in CBDA, and the phenolic –OH vibrational mode nearing the carboxylic acid group is further from the –CH stretching modes. This last result indicates that the presence of the carboxylic acid group in CBDA stabilizes this particular mode. Additionally, decarboxylation also results in the loss of the carbonyl stretching mode, leaving four resolved vibrational modes predicted at 1568, 1611, 1642, and 1683 cm^{-1} in the simulated spectrum of CBD. The first two correspond to two different breathing modes of the phenol ring, while the other two represent individual C═C stretching modes. While these modes were present in the simulated spectrum for CBDA, the carbonyl and two C═C stretching

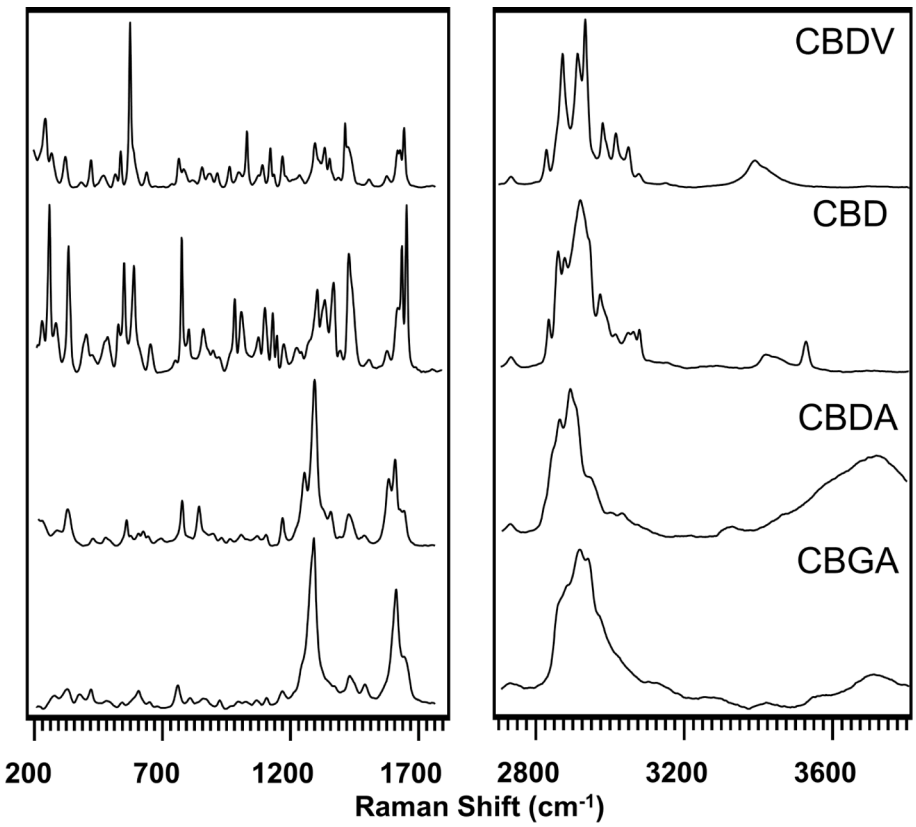

Fig. 4. Experimental Raman Spectra of CBD Pathway.

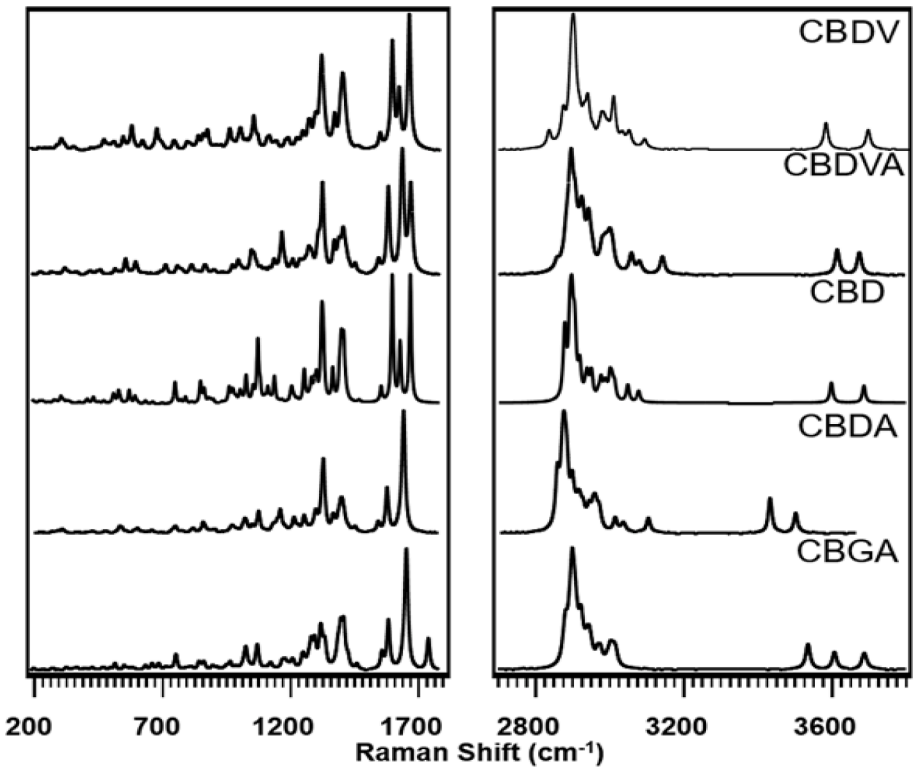

Fig. 5. Simulated Raman Spectra of CBD Pathway.

modes were indistinguishable, meaning the loss of the carbonyl group provided a greater energy difference in the two C═C stretching modes. The loss of the carboxylic acid group also cases an increase in intensity in the ring breathing mode, indicating that the carboxylic acid moiety hinders this particular motion. Aside from these differences, the fingerprint region is nearly identical while possessing greater peak intensities. Likewise, in the –CH stretching region, the only major difference between the two simulated spectra is greater peak separation and the presence of two additional peaks caused by band splitting not present in CBDA.

In the experimental spectra, CBD is shown to have greater peak intensities and less band broadening than that of CBDA. As predicted by theory, the –OH stretching modes of CBD are closer in energy, however unlike CBDA, these modes are red shifted as compared to their simulated counterparts. Much less band broadening is seen in CBD than CBDA, with the higher energy –OH stretching mode in particular being a distinct peak rather than a broad band. While the other –OH stretch still possesses some broadening, this decrease in band broadening suggests significantly fewer hydrogen bonding interactions, at least at the higher energy –OH group. In the –CH stretching region, much similarity is seen between CBD and CBDA, especially with regards to the overall shape and broad peak in the middle. There is, however, an additional resolved peak on the left side of the band, however given the increased band broadening of the CBDA spectrum, it is difficult to determine whether this is present there as well. When compared to theory, band broadening is shown to cause two peaks to merge into the largest peak seen in this region. Moving onto the C═C stretching and ring breathing modes, four peaks are identifiable, compared to three for CBDA. The small peak around 1680 cm^{-1} corresponds to a ring breathing mode not present in CBDA. In CBDA, the larger band possesses a shoulder on the right side, whereas in CBD this shoulder arises on the left. While simulations predict that the ring breathing mode will be more intense than the lower energy C═C stretching mode, experimentally the opposite occurs. In the rest of the fingerprint region, CBD's spectrum possesses overall much more intensity and peak separation than that for CBDA due to the crystalline nature of the substance.

As mentioned previously, CBDVA was not available for study at the time of this work. Therefore, comparisons can only be made between the simulated spectra of CBDVA and CBGA with the caveat that there is no experimental data to support or disprove such comparisons. It can be seen from the simulated spectrum in Fig. 5 that many of the spectral discrepancies between CBGA and CBDA are also present here. The –OH stretch in closest proximity to the carboxylic acid moiety is similar in energy to the –CH stretching modes, which is potentially due to internal hydrogen bonding like in CBDA, although experimental data would be necessary to prove this. Comparing the –CH stretching regions of CBGA and CBDVA, these results show that the –CH stretching modes' two highest energy peaks shown in the spectrum for CBDVA are not present in the spectra for CBGA, there is only one resolved peak to the right of this band in CBDVA's spectrum whereas CBGA's possesses two, and the peak shoulder on the left side of the band is lower in energy as well. As with CBDA, spectral differences potentially arise from the cyclization of the terpene tail into the monoterpene ring. The effective loss of an ethyl group in the hydrocarbon tail, and thus several –CH stretching modes, also potentially contributes to these discrepancies. The clearest predicted deviation from CBGA besides the –OH stretching modes occurs in the region containing carbonyl and C═C stretching modes. Although both simulated spectra feature four resolved peaks, predicted energies and intensities differ. For CBDVA as compared to CBGA, the carbonyl stretching mode undergoes a red shift and an increase in intensity, the terpenic C═C stretching mode is greater in energy than the carbonyl stretching mode, and the ring breathing modes' highest energy peak undergoes an increase in intensity. All of these spectral differences are potentially the result of intramolecular hydrogen bonding between the phenolic –OH group and the carboxylic acid group that decreases the energy of the carbonyl stretching mode, however experimental studies would be necessary to prove this.

CBDVA undergoes decarboxylation to form CBDV, which is shown to have multiple spectroscopic differences. In the simulated spectra, one fewer –OH vibrational mode is seen, and the –OH vibrational mode close

in energy to the –CH stretching region in CBDVA undergoes a blue shift to near the other –OH vibrational mode in CBDV, indicating that the carboxylic acid again has a stabilizing effect on this particular mode. Interestingly, the –CH stretching modes differ more than anticipated, with the overall –CH stretching band featuring two peaks to its left while CBDVA only possesses a mildly intense shoulder. To the right of this band, the spectrum for CBDVA features two peaks whereas the spectrum for CBDV shows only one, a discrepancy possibly resulting from the removal of the carboxylic acid group. The less intense middle band here only shows one peak for CBDVA while CBDV shows two, and the highest energy peak for CBDV is not found in the spectrum for CBDVA. In the absence of the carbonyl stretching mode, the two simulated C═C stretching modes have a greater energy difference between them, indicating that the removal of the carboxylic acid group also lowers the energy of the C═C stretching modes, increases the energy difference between them, and increases the intensity of the higher energy peak. This removal did not, however, have a noticeable impact on the ring breathing mode.

These predicted spectroscopic changes were largely verified by the experimental spectrum of CBDV. As predicted, the –OH modes blue shifted from CBDVA to CBDV, however instead of staying as two individual peaks, they combined to form a broad band centered at 3387 cm^{-1}, a red shift in energy compared to the simulated CBDV spectrum possibly caused by hydrogen bonding. Furthermore, the experimental CH stretching modes of CBDV are more separated than expected from theory, accentuating the changes in simulated spectra described above. The experimental spectrum also verified that the higher energy C═C stretching mode possesses a greater intensity than its lower energy counterpart (both of which red shifted compared to the simulated spectrum), however failed to show increased separation in energy.

3.3. THC pathway – Δ^9-THCA, Δ^9-THC, Δ^8-THC, and CBN

In this third pathway, CBGA converts to Δ^9-THCA via THCA synthase. From there, Δ^9-THCA decarboxylates into Δ^9-THC, which isomerizes to Δ^8-THC. Finally, Δ^9-THC oxidizes into CBN. The first step in this process leads to an effective loss of one OH functional group, removing a hydrogen so that the oxygen can bond to an additional carbon group. Experimental and simulated spectra of these species are shown in Figs. 6 and 7 respectively. The simulated spectrum illustrates this pathway, as there is a loss of one –OH vibrational band. The two remaining are greatly separated, indicating internal hydrogen bonding between the carbonyl oxygen and hydroxyl group similar to that seen in the other cannabinoids. However, this result is not observed experimentally, as there are no discernable –OH stretching peaks. Even though the experimental spectrum is the most resolved data collected for Δ^9-THCA over multiple attempts with several different samples, the –OH stretching region of the spectrum remains seemingly unresolved, suggesting that the hydrogen bonding activity of Δ^9-THCA is very strong.

In the –CH stretching region, while both spectra contain six peaks, the most intense peak is blue shifted while the entire band is red shifted in the experimental spectrum for Δ9-THCA as opposed to that of CBGA. Less peak separation is seen here, however this was not due to the nature of the sample as the Δ9-THCA sample was crystalline. The differences seen here can be attributed to the increase in cyclic rings present in Δ9-THCA. While good agreement between experiment and theory is seen in the –CH stretching region, the fingerprint region does not possess this quality. From simulation to experiment four peaks (1549, 1596, 1654, and 1668 cm^{-1}) become three (1593, 1619, and 1663 cm^{-1}) due to band broadening while also experiencing a red shift along with the experimental peak at 1294 cm^{-1}.

Moving on to Δ9-THC, an expected loss of an –OH stretch, caused by

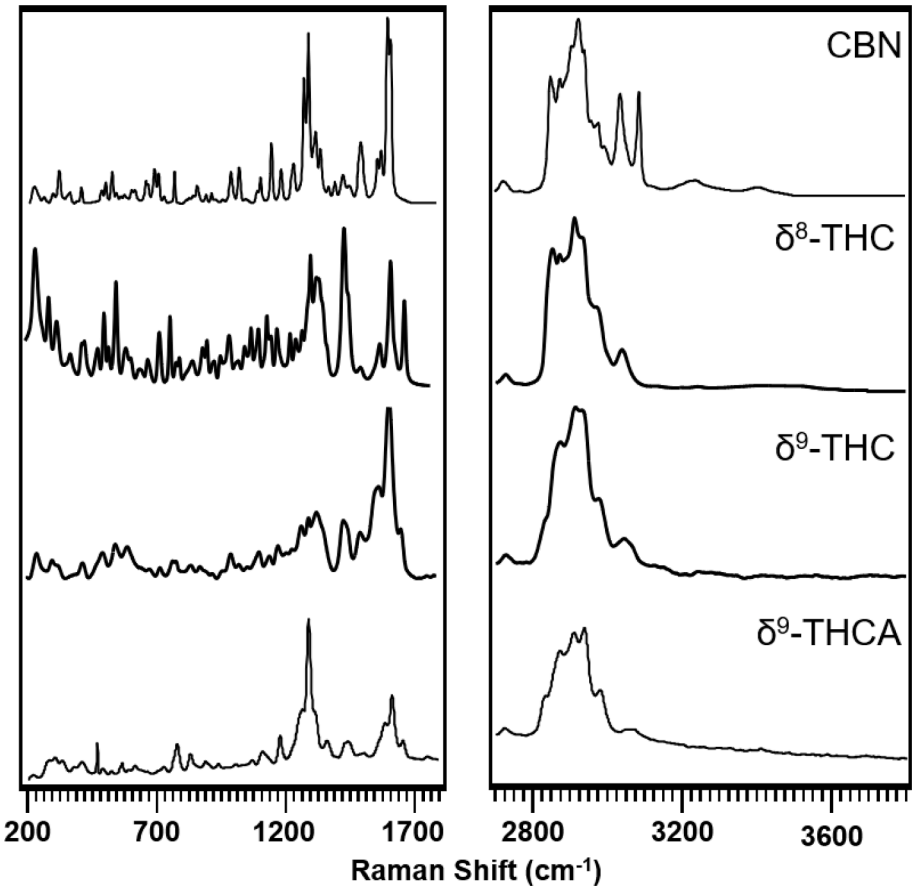

Fig. 6. Experimental Raman Spectra of THC Pathway.

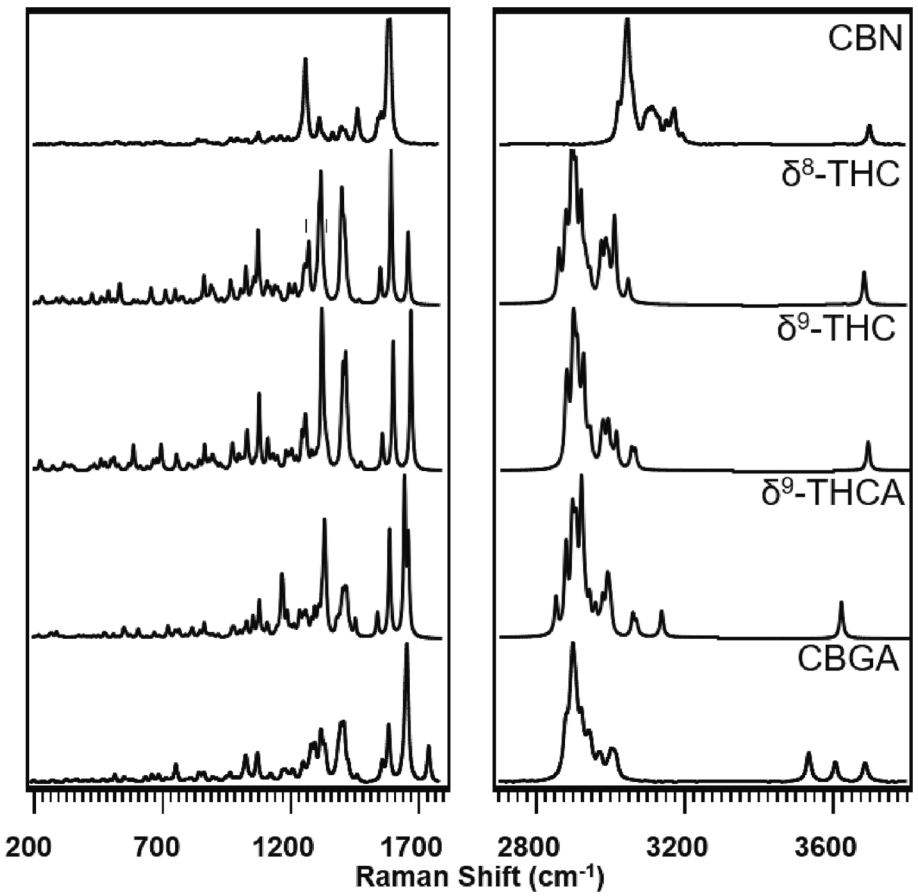

Fig. 7. Simulated Raman Spectra of THC Pathway.

the loss of the carboxylic acid group, is observed in the simulated spectrum. This leaves only one blue shifted –OH stretching vibrational mode, however as is the case with Δ9-THCA, this peak isn't observed experimentally, meaning it is not possible within the scope of this work to discuss potential hydrogen bonding effects. In the –CH stretching region however, higher peak separation is seen, allowing for better comparison. Three distinct groups of peaks are seen in both the simulated spectra of Δ^9-THCA and Δ^9-THC. A greater separation between the first and second groups is seen in the simulated spectrum of Δ^9-THC, and a slight red shift is seen in the second group. The similar appearance of this spectrum to that of Δ^9-THCA indicates the only change in –CH bonding occurs at the site of carboxylic acid loss and subsequent protonation.

Great similarity between the two simulated spectra occurs in the fingerprint region. Only minor differences occur, such as an increase in intensity of the peak at 1420 cm^{-1} and a merge in the two peaks closest to 17o0 cm^{-1} from Δ^9-THCA to Δ^9-THC. The latter reflects the loss of the C═O stretching mode due to thermal decarboxylation. However, this comparison loses its simplicity in the experimental data. Like with Δ^9-THCA, the peak separation in the red-shifted experimental spectrum is low compared to the simulated spectrum, so the best comparisons can be made for spectral data below 1700 cm^{-1}. In the simulated spectrum, the loss of C═O stretching modes is observed, however the only difference seen experimentally is a switch in peak intensity, with the lower energy group being more intense for Δ^9-THC. The lower peak separation is the main contributor to these disagreements, however like with Δ^9-THCA, the data presented here represents the most resolved data after several attempts with different samples. The lower peak separation is most likely caused by the inherent instability of the Δ^9-THC molecule. Because Δ^9-THC degrades relatively quickly when exposed to intense light and the ambient atmosphere, even given extreme caution in minimizing ambient light and performing the experiment in haste, it is possible the sample actively degraded over the course of the long scan time.

Since the only difference between Δ^9 and Δ^8-THC is the position of the double bond in the monoterpene ring, almost identical spectra are expected. The simulated spectra support this, with only minor differences between the two. From Δ^9-THC to Δ^8-THC, an increase in intensity is seen for the –CH stretching band at 3010 cm^{-1}. In the group of peaks just before 1700 cm^{-1}, the highest intensity peak becomes the middle peak rather than the one with the highest energy. This highest energy peak corresponds to C═C stretching in the monoterpene ring, while the middle peak corresponds to aromatic ring breathing in the phenolic ring. Beyond this, the fingerprint regions and –OH stretching region are nearly identical in the simulated spectra.

Experimentally, greater peak separation is seen when comparing Δ^8-THC to Δ^9-THC. Specifically, for the peaks associated with C═C stretching, the poorly separated peaks for Δ^9-THC become not only become more separated for Δ^8-THC, but also are in near perfect agreement with the simulated bands, possibly resulting from the change in double bond position: the experimental values are 1581, 1622, and 1676 cm^{-1}, while the simulated values are 1566, 1610, 1678 cm^{-1}. Compared to the simulated spectrum, however, imperfections can be seen. In the –CH stretching band, eight peaks can be seen in the simulated spectrum compared to only six in the experimental spectrum. As with the other cannabinoids, the hydrocarbon tail bound to the phenolic ring can rotate independently of the rest of the molecule, potentially causing band broadening due to increased rotational freedom. The broadness of the –OH vibrational band with a maximum intensity at 3424 cm^{-1} indicates the presence of hydrogen bonding, however the red shift (as compared to theory) and low intensity indicates the extent of these interactions is small. Due to the low peak separation of Δ^9-THC's

experimental spectrum, no true comparison can be made here.

Δ^9-THC and Δ^8-THC oxidize to form CBN, resulting in increased aromaticity of the monoterpene ring. The simulated spectrum of CBN shows major differences between the three simulated spectra in the C═C stretching and ring breathing modes. However, these modes don't possess great peak separation in CBN unlike Δ^8-THC. Instead, one major peak arises at 1600 cm^{-1} with a barely resolved shoulder on the left side, indicating that ring breathing in the second aromatic ring replaces the individual C═C stretching mode, creating one singular intense peak. In the –CH stretching region, the first peak in the overall band is narrower and the first two peaks are less resolved due to the removal of four hydrogens during oxidation. In the –OH stretching mode, much similarity is seen, including minimal difference in Raman shift and similar intensities.

The experimental spectrum for CBN reveals an overall good agreement between experiment and theory. In fact, increased peak separation is seen in the experimental spectrum. Intense peaks at 1610 and 1270 cm^{-1} both blue shift and split into two distinct peaks, along with many others in the fingerprint region. Unlike the other cannabinoid experimental spectra, this high peak separation extends into the –CH stretching region, even if there is some broadening of the overall band. Further divergence from theory is seen in the –OH stretching region. Where the simulated spectrum shows a narrow band with one peak, the experimental spectrum features a red-shifted broad band with two peaks. A red shift this large could potentially indicate fewer hydrogen bonding interactions, however other inter- or intramolecular interactions could be responsible. Additionally, the splitting of the peak suggests Fermi resonance which is typically not well predicted with computational methods.

3.4. CBC pathway – CBCA and CBC

Since CBCA was not available for study, comparisons can only be made between the simulated spectra of CBCA and CBGA. Experimental and simulated spectra are shown in Figs. 8 and 9 for these products. In the –OH stretching region, these spectra show two –OH vibrational modes for CBCA versus CBGA's three. Like the other first derivatives before it, the phenolic –OH vibrational mode for CBCA is closer in energy to the –CH modes, again likely due to the orientation of the phenolic –OH close to the carbonyl oxygen which leads to intramolecular hydrogen bonding and the stabilization of this particular vibrational mode. In the –CH stretching region, only minor spectroscopic changes are expected. A new three-peak band between the –CH modes and the phenolic –OH mode presents itself, and decreased peak separation is seen for the principal peak in this region, again possibly arising from increased cyclization. In the C═C and ring breathing region, clear differences between CBGA and CBCA arise. The ring breathing mode sees an increase in intensity, the carbonyl stretching mode undergoes a red shift, and five resolved peaks are present as opposed to CBGA's four. Here, different functional groups adjacent to these C═C bonds in the terpene tail create increased peak separation when contrasted with CBGA's similar groups.

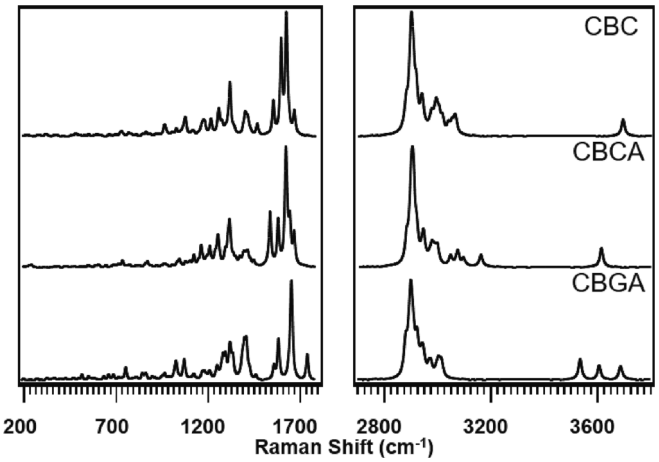

Fig. 9. Experimental Raman Spectra of CBC Pathway.

Finally, with regards to CBC, very good agreement between experiment and theory is seen that validates some discrepancies seen in the simulated spectrum for CBCA. Comparing the simulated spectra of CBC and CBCA, it is first seen that CBC possesses only one –OH vibrational mode compared to CBCA's two, which is expected due to the decarboxylation that turns CBCA into CBC. This removal of the carboxylic acid moiety also causes a blue shift in this mode, again suggesting that the carboxylic acid group stabilizes the phenolic –OH vibrational mode. In the –CH stretching modes, no drastic change is observed, which is expected due to the structural similarity between CBCA and CBC. The only notable differences occur in the two bands of higher energy than the most intense of the bunch, where the less energetic has three resolved peaks in CBC compared to two in CBCA and the more energetic has three in CBC and two in CBCA. Like before, this is most likely due to the increase in –CH functional groups due to protonation at the site of decarboxylation. In the fingerprint region, four peaks are observed for CBC in the carbonyl, C═C, and ring breathing region as opposed to CBCA's five. Unlike with the other cannabinoids, no appreciable effect on intensity and energy is seen for the C═C modes due to decarboxylation, however all major changes occur in the ring breathing modes, with the lower energy mode decreasing in intensity while its more

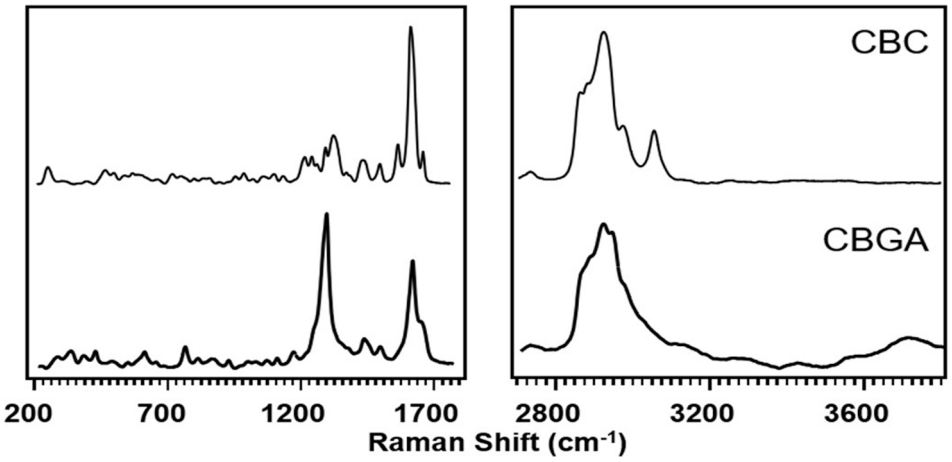

Fig. 8. Experimental Raman Spectra of CBC Pathway.

energetic counterpart increases in intensity.

The experimental spectrum of CBC validates the vast majority of these computational results. In the fingerprint region, the higher energy C═C and lower energy ring breathing modes are of comparable energy and intensity to their simulated analogs, with the only major discrepancy being a much smaller energy gap, and thus less peak separation, between the two. In the –CH stretching region, some spectral differences can be identified. In the experimental spectrum, the most intense peak in the band has two distinguishable shoulders on the left side, whereas the simulated spectra for CBC and CBCA showcase only one. This is potentially caused by a higher observed intensity in the peak located to the right of this most intense band, but due to the broadness of this experimental mode, the causality is difficult to discern. Furthermore, the band located at 3052 cm^{-1} in the experimental spectrum only has one resolved peak, whereas the simulated spectra for CBC and CBCA have two and three, respectively. The middle band in this region is clearly resolved in the simulated spectrum of CBC, however it remains difficult to resolve experimentally. Finally, in the –OH stretching region, the spectral data is extremely difficult to resolve. It is possible that like with Δ^8-THC, this the band is extremely broad and weak, but instrumental noise could also be the cause. If it is indeed a band, the extreme broadness would indicate major hydrogen bonding interactions. Due to the lack of experimental data for CBCA, it is unknown how the vibrational modes in each of these regions would compare to that of CBC, however it is theorized that the –OH stretching band possibly seen here would possess a much greater intensity and energy.

4. Conclusions

The data presented in this work represents the most resolved experimental and highest level simulated spectra available to date for each cannabinoid. The derivatives of CBGA often display higher peak separation in the experimental spectra than CBGA itself, which is most likely attributable to physical composition of the samples. The overall agreement between the experimental and simulated spectra is good, however for certain vibrational modes, especially those in the –OH stretching region, deviations are observed most likely due to hydrogen bonding. That being said, the most evident spectroscopic changes are observed in this region, especially when transitioning from an acidic to a decarboxylated cannabinoid, making the OH stretching region a good probe for decarboxylation reactions. Although not as evident, spectroscopic differences are also identified in the C═C stretching and ring breathing modes, mostly occurring from the loss of a C═O stretching mode due to decarboxylation.

Future work should investigate hydrogen bonding interactions in the acidic cannabinoids, especially the possibility of internal hydrogen bonding between the phenolic OH and carbonyl oxygen, and how it affects the vibrational energy levels. Finally, further computational studies could investigate the different isomeric forms for each cannabinoid to determine if there is an appreciable difference in their simulated spectra.

CRediT authorship contribution statement

Trevor J. Wolfe: Data Curation, formal analysis, Methodology, Writing: original draft. Nicholas A. Kruse: Data Curation, formal analysis, Methodology, Writing: original draft, Writing: Review & Editing. Kalee N. Sigworth: Data Curation, formal analysis, Methodology, Writing: Review & Editing. **Mohamed M. Radwan:** Methodology, Writing: Review & Editing. **Amira S. Wanas:** Methodology, Writing: Review & Editing. **Mahmoud A. ElSohly:** Methodology, Project Administration, Resources, Supervision, Writing: Review & Editing. **Nathan I. Hammer:** Conceptualization, formal analysis, Funding Acquisition, Investigation, Project Administration, Resources, Supervision, Writing: Review & Editing.

Declaration of Competing Interest

The authors declare that they have no known competing financial interests or personal relationships that could have appeared to influence the work reported in this paper.

Data availability

Data will be made available on request.

Acknowledgments

We are grateful for financial support from the National Science Foundation under grant number OIA-1757220.

Appendix A. Supplementary data

Supplementary data to this article can be found online at https://doi.org/10.1016/j.saa.2023.123133.

References

[1] R.M. Murray, P.D. Morrison, C. Henquet, M.D. Forti, Cannabis, the mind and society: the hash realities, Nat. Rev. Neurosci. 8 (11) (2007) 885–895.
[2] M. Mostafaei Dehnavi, A. Ebadi, A. Peirovi, G. Taylor, S.A. Salami, THC and CBD Fingerprinting of an Elite Cannabis Collection from Iran: Quantifying Diversity to Underpin Future Cannabis Breeding, Plants 11 (2022) 129.
[3] M.E. Eggers, Y.O. Lee, K. Jackson, J.L. Wiley, L. Porter, J.M. Nonnemaker, Youth use of electronic vapor products and blunts for administering cannabis, Addict. Behav. 70 (2017) 79–82.
[4] C.D. Delnevo, M. Hrywna, The relationship of cigars, marijuana, and blunts to adolescent bidi use, Public health reports (Washington, D.C. : 1974), 121 (2006) 603-608.
[5] S. Steigerwald, P.O. Wong, B.E. Cohen, J.H. Ishida, M. Vali, E. Madden, S. Keyhani, Smoking, Vaping, and Use of Edibles and Other Forms of Marijuana Among U.S. Adults, Annals of Internal Medicine, 169 (2018) 890-892.
[6] R. Clarke, D. Watson, Cannabis and Natural Cannabis Medicines, 2007, pp. 1-15.
[7] O. Aizpurua-Olaizola, J. Omar, P. Navarro, M. Olivares, N. Etxebarria, A. Usobiaga, Identification and quantification of cannabinoids in Cannabis sativa L. plants by high performance liquid chromatography-mass spectrometry, Anal. Bioanal. Chem. 406 (29) (2014) 7549–7560.
[8] M.A. ElSohly, D. Slade, Chemical constituents of marijuana: The complex mixture of natural cannabinoids, Life Sci. 78 (5) (2005) 539–548.
[9] I.J. Flores-Sanchez, R. Verpoorte, Secondary metabolism in cannabis, Phytochem. Rev. 7 (3) (2008) 615–639.
[10] F. Degenhardt, F. Stehle, O. Kayser, Chapter 2 - The Biosynthesis of Cannabinoids, in: V.R. Preedy (Ed.), Handbook of Cannabis and Related Pathologies, Academic Press, San Diego, 2017, pp. 13–23.
[11] A. Helander, M. Johansson, A. Andersson, T. Villén, Analytical and medico-legal problems linked to the presence of delta-8-tetrahydrocannabinol (delta-8-THC): Results from urine drug testing in Sweden, Drug Test. Anal. 14 (2022) 371–376.
[12] K. Johnson-Arbor, S. Smolinske, The current state of delta-8 THC, Am. J. Emerg. Med. 56 (2022) 259–261.
[13] E. Crocioni, Raman spectroscopy of Cannabis Sativa trichomes and selected cannabinoids, 2021.
[14] L. Sanchez, C. Filter, D. Baltensperger, D. Kurouski, Confirmatory non-invasive and non-destructive differentiation between hemp and cannabis using a hand-held Raman spectrometer, RSC Adv. 10 (2020) 3212–3216.
[15] L. Sanchez, D. Baltensperger, D. Kurouski, Raman-Based Differentiation of Hemp, Cannabidiol-Rich Hemp, and Cannabis, Anal. Chem. 92 (2020) 7733–7737.
[16] K. Sigworth, Raman Spectroscopy Study of Delta-9-Tetrahydrocannabinol and Cannabidiol and their Hydrogen-Bonding Activities, University of Mississippi Honors Thesis, 2020.
[17] K. Sivashanmugan, K. Squire, A. Tan, Y. Zhao, J.A. Kraai, G.L. Rorrer, A.X. Wang, Trace Detection of Tetrahydrocannabinol in Body Fluid via Surface-Enhanced Raman Scattering and Principal Component Analysis, ACS Sensors 4 (4) (2019) 1109–1117.
[18] K. Sivashanmugan, Y. Zhao, A.X. Wang, Tetrahydrocannabinol Sensing in Complex Biofluid with Portable Raman Spectrometer Using Diatomaceous SERS Substrates, Biosensors 9 (2019) 125.
[19] S. Farquharson, C. Brouillette, W. Smith, C. Shende, A Surface-Enhanced Raman Spectral Library of Important Drugs Associated With Point-of-Care and Field Applications, Front. Chem. 7 (2019).
[20] S. Yüksel, A.M. Schwenke, G. Soliveri, S. Ardizzone, K. Weber, D. Cialla-May, S. Hoeppener, U.S. Schubert, J. Popp, Trace detection of tetrahydrocannabinol (THC) with a SERS-based capillary platform prepared by the in situ microwave synthesis of AgNPs, Anal. Chim. Acta 939 (2016) 93–100.

[21] S.K. Islam, Y.P. Cheng, R.L. Birke, M.V. Cañamares, C. Muehlethaler, J. R. Lombardi, An analysis of tetrahydrocannabinol (THC) and its analogs using surface enhanced Raman Scattering (SERS), Chem. Phys. 536 (2020), 110812.
[22] V.M. Moreno, M. López-López, J.-C. Atoche, C. García-Ruiz, Raman identification of drug of abuse particles collected with colored and transparent tapes, Sci. Justice 54 (2014) 164–169.
[23] S. Fedchak, Presumptive field testing using portable raman spectroscopy, Office of Justice Programs, Document No.: 244564, 2014.
[24] C. Deriu, I. Conticello, A.M. Mebel, B. McCord, Micro Solid Phase Extraction Surface-Enhanced Raman Spectroscopy (μ-SPE/SERS) Screening Test for the Detection of the Synthetic Cannabinoid JWH-018 in Oral Fluid, Anal. Chem. 91 (2019) 4780–4789.
[25] J. Omar, B. Slowikowski, C. Guillou, F. Reniero, M. Holland, A. Boix, Identification of new psychoactive substances (NPS) by Raman spectroscopy, J. Raman Spectrosc. 50 (2019) 41–51.
[26] A. Giorgetti, L. Mogler, B. Haschimi, S. Halter, F. Franz, F. Westphal, S. Fischmann, J. Riedel, M. Pütz, V. Auwärter, Detection and phase I metabolism of the 7-azaindole-derived synthetic cannabinoid 5F-AB-P7AICA including a preliminary pharmacokinetic evaluation, Drug Test. Anal. 12 (1) (2020) 78–91.
[27] T. Mostowtt, B. McCord, Surface enhanced Raman spectroscopy (SERS) as a method for the toxicological analysis of synthetic cannabinoids, Talanta 164 (2017) 396–402.
[28] S. Halter, B. Pulver, M. Wilde, B. Haschimi, F. Westphal, J. Riedel, M. Pütz, T. Schönberger, S. Stoll, J. Schäper, V. Auwärter, Cumyl-CBMICA: A new synthetic cannabinoid receptor agonist containing a cyclobutyl methyl side chain, Drug Test. Anal. 13 (1) (2021) 208–216.
[29] L. Zhang, G. Li, Handheld raman spectrometer for the rapid determination of synthetic cannabinoids, J. Forensic Sci. Med. 5 (2019) 29–32.
[30] S. Metternich, S. Fischmann, S. Münster-Müller, M. Pütz, F. Westphal, T. Schönberger, M. Lyczkowski, S. Zörntlein, C. Huhn, Discrimination of synthetic cannabinoids in herbal matrices and of cathinone derivatives by portable and laboratory-based Raman spectroscopy, Forensic Chem. 19 (2020) 100241.
[31] J. Calvo-Castro, A. Guirguis, E.G. Samaras, M. Zloh, S.B. Kirton, J. Stair, Jacqueline L. Stair, Detection of newly emerging psychoactive substances using Raman spectroscopy and chemometrics, RSC Advances 8 (56) (2018) 31924–31933.
[32] D.S. Burr, W.L. Fatigante, J.A. Lartey, W. Jang, A.R. Stelmack, N.W. McClurg, J. M. Standard, J.R. Wieland, J.-H. Kim, C.C. Mulligan, J.D. Driskell, Integrating SERS and PSI-MS with Dual Purpose Plasmonic Paper Substrates for On-Site Illicit Drug Confirmation, Anal. Chem. 92 (9) (2020) 6676–6683.
[33] R.S. Borges, A.B.F. da Silva, Chapter e12 - Cannabidiol as an Antioxidant, in: V. R. Preedy (Ed.), Handbook of Cannabis and Related Pathologies, Academic Press, San Diego, 2017, pp. e122–e130.
[34] Ş. Toprak, Theoretical calculation of some chemical properties of the cannabidiol (CBD) molecule, Int. J. Sci. Lett. 3 (2) (2021) 129–142.
[35] A. Kumer, N. Sarker, S. Paul, A. Zannat, The Theoretical Prediction of Thermophysical properties, HOMO, LUMO, QSAR and Biological Indics of Cannabinoids (CBD) and Tetrahhdrocannabinol (THC) by Computational Chemistry, Adv. J. Chem.-Sect. A 2 (2019) 190–202.
[36] H. Boulebd, D.M. Pereira, I. Amine Khodja, N.T. Hoa, A. Mechler, Q.V. Vo, Assessment of the free radical scavenging potential of cannabidiol under physiological conditions: Theoretical and experimental investigations, J. Mol. Liq. 346 (2022) 118277.
[37] V.A.N. Bragança, T.G. França, A.C.S.P.S. de Jesus, I.C. Palheta, F.P.A. Melo, P.A.P. F.G. Neves, A.B. Lima, R.S. Borges, Impact of conformational and solubility properties on psycho-activity of cannabidiol (CBD) and tetrahydrocannabinol (THC), Chem. Data Collections 26 (2020), 100345.
[38] A. Garcia, Computational Chemistry, Drug Design, and Drug Re-Discovery Aimed at Theory-Directed Synthesis of Cannabinoids and Computational Methods to Predict Bioactivity from Ligand Structure. Department of Chemistry, University of California, Riverside, 2012.
[39] J. Vacek, J. Vostalova, B. Papouskova, D. Skarupova, M. Kos, M. Kabelac, J. Storch, Antioxidant function of phytocannabinoids: Molecular basis of their stability and cytoprotective properties under UV-irradiation, Free Radic. Biol. Med. 164 (2021) 258–270.
[40] J.S. de Castro, C.H.P. Rodrigues, A.T. Bruni, In Silico Infrared Characterization of Synthetic Cannabinoids by Quantum Chemistry and Chemometrics, J. Chem. Inf. Model. 60 (2020) 2100–2114.
[41] M.N. Sarker, A. Kumer, M.J. Islam, S. Paul, A computational study of thermophysical, HOMO, LUMO, vibrational spectrum and UV-visible spectrum of cannabicyclol (CBL), and cannabigerol (CBG) using DFT, Asian J. Nanosci. Mater. 2 (2019) 439–447.
[42] M. Alkaseem, M. Baron, SERS and DFT study of 5F-PB-22, J. Raman Spectrosc. 49 (10) (2018) 1594–1606.
[43] P. Verma, D.G. Truhlar, Status and Challenges of Density Functional Theory, Trends Chem. 2 (4) (2020) 302–318.
[44] S.A. Ahmed, S.A. Ross, D. Slade, M.M. Radwan, F. Zulfiqar, M.A. ElSohly, Cannabinoid Ester Constituents from High-Potency Cannabis sativa, J. Nat. Prod. 71 (4) (2008) 536–542.
[45] M. Radwan, S. Ross, D. Slade, S. Ahmed, F. Zulfiqar, M. ElSohly, Isolation and Characterization of New Cannabis Constituents from a High Potency Variety, Planta Med 74 (3) (2008) 267–272.
[46] A.S. Husni, C.R. McCurdy, M.M. Radwan, S.A. Ahmed, D. Slade, S.A. Ross, M. A. ElSohly, S.J. Cutler, Evaluation of phytocannabinoids from high-potency Cannabis sativa using in vitro bioassays to determine structure–activity relationships for cannabinoid receptor 1 and cannabinoid receptor 2, Med. Chem. Res. 23 (2014) 4295–4300.
[47] P. Marzullo, F. Foschi, D.A. Coppini, F. Fanchini, L. Magnani, S. Rusconi, M. Luzzani, D. Passarella, Cannabidiol as the Substrate in Acid-Catalyzed Intramolecular Cyclization, J. Nat. Prod. 83 (2020) 2894–2901.
[48] M.J. Frisch, G.W. Trucks, H.B. Schlegel, G.E. Scuseria, M.A. Robb, J.R. Cheeseman, G. Scalmani, V. Barone, G.A. Petersson, H. Nakatsuji, X. Li, M. Caricato, A.V. Marenich, J. Bloino, B.G. Janesko, R. Gomperts, B. Mennucci, H.P. Hratchian, J.V. Ortiz, A.F. Izmaylov, J.L. Sonnenberg, Williams, F. Ding, F. Lipparini, F. Egidi, J. Goings, B. Peng, A. Petrone, T. Henderson, D. Ranasinghe, V.G. Zakrzewski, J. Gao, N. Rega, G. Zheng, W. Liang, M. Hada, M. Ehara, K. Toyota, R. Fukuda, J. Hasegawa, M. Ishida, T. Nakajima, Y. Honda, O. Kitao, H. Nakai, T. Vreven, K. Throssell, J.A. Montgomery Jr., J.E. Peralta, F. Ogliaro, M.J. Bearpark, J.J. Heyd, E.N. Brothers, K.N. Kudin, V.N. Staroverov, T.A. Keith, R. Kobayashi, J. Normand, K. Raghavachari, A.P. Rendell, J.C. Burant, S.S. Iyengar, J. Tomasi, M. Cossi, J.M. Millam, M. Klene, C. Adamo, R. Cammi, J.W. Ochterski, R.L. Martin, K. Morokuma, O. Farkas, J.B. Foresman, D.J. Fox, Gaussian 16 Rev. C.01, in, Wallingford, CT, 2016.
[49] Y. Zhao, D.G. Truhlar, The M06 suite of density functionals for main group thermochemistry, thermochemical kinetics, noncovalent interactions, excited states, and transition elements: two new functionals and systematic testing of four M06-class functionals and 12 other functionals, Theor. Chem. Acc. 120 (2008) 215–241.
[50] T. Kupka, M. Stachów, M. Nieradka, J. Kaminsky, T. Pluta, S.P.A. Sauer, From CCSD(T)/aug-cc-pVTZ-J to CCSD(T) complete basis set limit isotropic nuclear magnetic shieldings via affordable DFT/CBS calculations, Magn. Reson. Chem. 49 (2011) 231–236.